APL Photonics

Solitonic supercontinuum of femtosecond mid-IR pulses in W-type index tellurite fibers with two zero dispersion wavelengths

Cite as: APL Photonics 1, 086101 (2016); https://doi.org/10.1063/1.4958333
Submitted: 04 April 2016 • Accepted: 28 June 2016 • Published Online: 18 November 2016

S. Kedenburg, T. Steinle, F. Mörz, et al.

APL PHOTONICS **1**, 086101 (2016)

Solitonic supercontinuum of femtosecond mid-IR pulses in W-type index tellurite fibers with two zero dispersion wavelengths

S. Kedenburg,[1,a] T. Steinle,[1] F. Mörz,[1] A. Steinmann,[1] D. Nguyen,[2] D. Rhonehouse,[2] J. Zong,[2] A. Chavez-Pirson,[2] and H. Giessen[1]
[1]*4th Physics Institute and Research Center SCOPE, University of Stuttgart, 70550 Stuttgart, Germany*
[2]*NP Photonics, 9030 South Rita Road, Suite 120, Tucson, Arizona 85747, USA*

(Received 4 April 2016; accepted 28 June 2016; published online 22 August 2016)

We present a detailed experimental parameter study on mid-IR supercontinuum generation in W-type index tellurite fibers, which reveals how the core diameter, pump wavelength, fiber length, and pump power dramatically influence the spectral broadening. As pump source, we use femtosecond mid-IR pulses from a post-amplified optical parametric oscillator tunable between 1.7 μm and 4.1 μm at 43 MHz repetition rate. We are able to generate red-shifted dispersive waves up to a wavelength of 5.1 μm by pumping a tellurite fiber in the anomalous dispersion regime between its two zero dispersion wavelengths. Distinctive soliton dynamics can be identified as the main broadening mechanism resulting in a maximum spectral width of over 2000 nm with output powers of up to 160 mW. We experimentally demonstrated that efficient spectral broadening with considerably improved power proportion in the important first atmospheric transmission window between 3 and 5 μm can be achieved in robust W-type tellurite fibers pumped at long wavelengths by ultra-fast lasers. [http://dx.doi.org/10.1063/1.4958333]

I. INTRODUCTION

High-power single-mode fiber-based supercontinuum sources with extremely wide wavelength coverage are ideal sources for spectroscopy and metrology as well as for defense applications.[1] To cover the mid-infrared spectral region where several molecular vibrations of relevant organic compounds are located (molecular fingerprint region 2-20 μm[2]) alternative materials to standard silica optical fibers have to be utilized due to high absorption losses in fused silica above a wavelength of 2.4 μm. Particularly, high-power supercontinuum generation in the mid-infrared based on soft glasses[1,3,4] with higher nonlinearities and wider transparency windows such as chalcogenide[6–9] and fluoride fibers[10] have been reported. A further interesting material is tellurite glass with a one order of magnitude higher nonlinear refractive index compared to fused silica and an excellent optical transparency up to 5 μm.[5] Furthermore, tellurium oxide based glasses exhibit good mechanical robustness and chemical durability superior to that of chalcogenides and fluorides. They therefore possess a high optical damage threshold[1] on the order of ~15-20 GW/cm^2.

Most reports about tellurite glass fibers in the literature have been based on microstructured optical fibers pumped in the near-IR.[11–15] These fibers show enhanced nonlinearities due to the small core sizes and engineered zero dispersion wavelengths (ZDWs) below 2 μm, allowing for anomalous dispersion pumping with conventional laser systems. However, the enormous design flexibility to tailor the nonlinearity and the dispersion profile comes along with a limited spectral coverage of the wavelength region above 3 μm.[11–14] This is due to increased absorption related to

[a]s.kedenburg@pi4.uni-stuttgart.de

water retention and a reduced damage threshold which hinders further power scaling. An improvement in the spectral coverage has been achieved by Domachuk *et al.*,[15] reporting supercontinuum generation up to 4.8 μm in 8 mm of highly nonlinear tellurite microstructured fiber. The spectral bandwidth at an output power of 70 mW was over 4000 nm, but the power proportion in the mid-IR region remains small because of a pump wavelength in the near-IR around 1.5 μm.

However, the investigation of more robust and transparent step-index fibers (W-type refractive index profile) has been limited to one experimental study in the picosecond regime by Thapa *et al.*[16] and another numerical work in the femtosecond regime by Wei *et al.*[17] The simple W-type index structure also allows for tailoring the ZDW accordingly with the advantage of a solid cladding that provides superior power scaling properties compared to microstructured fibers.[17] Furthermore, this fiber type is suitable for an all-fiber system because it can be fusion spliced to standard step-index silica fiber. With a Tm-doped fiber amplifier as pump source, a supercontinuum covering the 1.3-4.5 μm region has been generated with a high output power of 1.2 W, half of which corresponded to wavelengths longer than 2 μm.[16] The authors managed to develop a tellurite glass with ultra-low losses of less than 0.5 dB/m in the transmission window from 0.6 to 4.5 μm.[18] However, in the numerical investigation of Ref. 17 the authors proposed to pump a W-type tellurite fiber with ultra-fast laser sources in the mid-IR at a wavelength of around 3 μm to generate supercontinua with a high power proportion in the 3-5 μm atmospheric window.

In this letter, we investigate the spectral behavior of supercontinua experimentally and numerically by launching mid-IR fs-pulses into simple, ultra-low loss, and very robust W-type index tellurite fibers. When pumped in the anomalous dispersion regime between the two ZDWs, the solitonic broadening could be enhanced by the generation of red-shifted dispersive waves (DW) in the normal dispersion range on the long-wavelength side above the second ZDW.

Compared to a recently published work by Gauthier *et al.*[19] where they pumped a fluoroindate fiber by a 2 kHz erbium-doped fiber amplifier with a pulse duration of about 600 ps our approach has several benefits. Firstly, to generate a supercontinuum with a high coherence, the pump source needs to operate in the femtosecond regime since picosecond pumping is detrimental as shown in Ref. 20. Furthermore, a low repetition rate (kHz level) compared to tens of MHz has some disadvantages regarding, e.g., incompatibility to fast-scanning FTIR spectrometers. In terms of average output power we achieved up to 160 mW, compared to their 16 mW,[19] which is better by a factor of 10 with the advantage of further power scalability due to the excellent mechanical properties of our fiber.

II. PROPERTIES OF THE W-TYPE INDEX TELLURITE FIBER

A W-type fiber is composed of three different refractive index regions: core, inner cladding, and outer cladding.[21] The core has the largest refractive index of the three, and the outer cladding index is the next largest as can be seen in Fig. 1(a). The advantages of such a doubly clad fiber are a tight confinement of the mode within the core, a flattened dispersion profile with good control of the locations of the two ZDWs, and a larger possible core area for single mode operation compared to a common singly clad fiber. The tightly confined mode and hence, a high fraction of mode power that propagates in the core help to reduce optical losses. The dual ZDW feature results in a partial flattening of the dispersion curve in the region between these two wavelengths as shown in Fig. 1(b). The benefit of a larger possible core diameter helps to lower the coupling losses while still operating under single-mode condition up to a higher V-parameter ($V = 3.8$) than in conventional step-index fibers[21] (see Fig. 1(c)). However, the mode power can leak into the outer cladding due to a smaller effective refractive index of the core and inner cladding.[22] This effect leads to a catastrophic loss for the mode and can occur when the operating wavelength, and hence, the mode field radius, become too large. Therefore, an effective cutoff wavelength λ_f exists,[23,24] such that operation is restricted between this value and the single-mode cutoff-wavelength λ_c, that is, $\lambda_c < \lambda < \lambda_f$. Our tellurite fibers had core diameters of 3.2 μm, 4.2 μm, and 5.0 μm and a numerical aperture of about 0.56.[16] With a three times larger inner cladding diameter than the core and the refractive index differences given in Fig. 1(a) the leakage cutoff-wavelengths λ_f occur at a V-parameter of around $V = 1.4$[23,24] (see Fig. 1(c)). The first ZDWs remain nearly fixed for all core diameters and are located at around

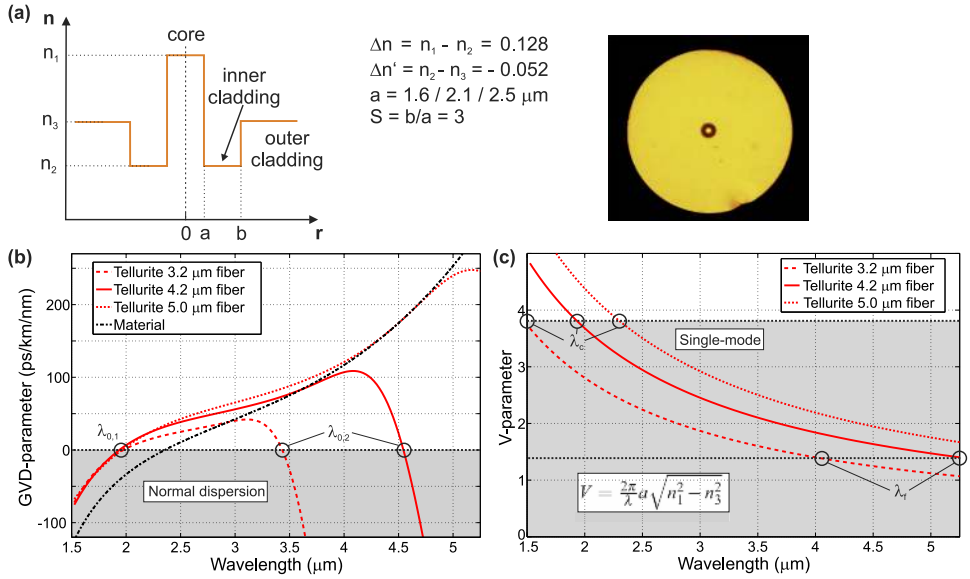

FIG. 1. (a) Refractive index profile, fiber parameters, and microscope image of the fiber end-face of the W-type tellurite fibers.[16] (b) Calculated group velocity dispersion (GVD) of the fundamental mode for W-type index tellurite fibers with core diameters of 3.2 μm, 4.2 μm, and 5.0 μm (red) in comparison with the material dispersion of tellurite glass (black dashed line). The zero dispersion boundary is marked with a black dotted line with anomalous dispersion between $\lambda_{0,1}$ and $\lambda_{0,2}$. The second ZDW can be tailored accordingly through a change of the core diameter. (c) Calculated V-parameter for the W-type index tellurite fibers with single-mode cutoff-wavelengths at λ_c, and cutoff-wavelengths due to leakage losses at λ_f. The single-mode boundary at $V = 3.8$ and the leakage boundary at $V = 1.4$ are marked with black dotted lines.

$\lambda_{0,1}$ = 1.9 μm. The second ZDWs increase with the core diameter and are located at $\lambda_{0,2} \approx 3.5$ μm, $\approx$4.6 μm, and >5.5 μm, respectively. Between these two ZDWs the fiber exhibits anomalous dispersion, and soliton dynamics play the dominant role during spectral broadening. Increased material absorption of tellurite glass above a wavelength of 4.5 μm[16] can limit the spectral broadening on the longer wavelength side.

III. EXPERIMENTAL SETUP

Figure 2 illustrates a schematic of the experimental setup. A home-built 7 W Yb:KGW oscillator[25] with a pulse duration of 500 fs, a repetition rate of 43 MHz, and a central wavelength of 1.03 μm was used to pump a fiber-feedback optical parametric oscillator (OPO).[26,27] The signal pulses with a duration of 250-500 fs at full width at half maximum were further amplified with an optical parametric amplifier (OPA),[28] delivering gap free tunable pulses between 1.4 and 4.1 μm with a maximum average output power of around 0.7 W at a wavelength of 3.2 μm. The separation of signal and idler after the crystal was achieved with broadband long- and short-pass filters. Both signal (1.7 μm) and idler (2.5 μm-4.1 μm) of the post amplifier with pulse durations between 280

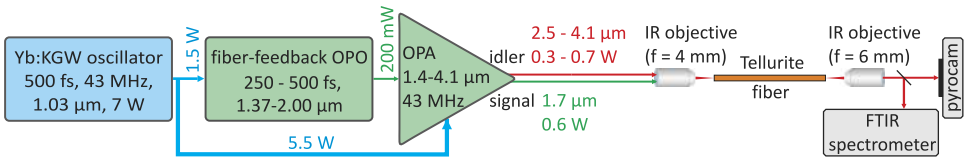

FIG. 2. Schematic of the experimental setup. A home-built Yb:KGW oscillator was used to pump a fiber-feedback OPO whose signal pulses were applied to seed an OPA. Both signal (1.7 μm) and idler (2.5 μm-4.1 μm) of the post amplifier were used to couple into the W-type index tellurite fibers via an aspherical lens. Coupling into the 3.2 μm–5.0 μm large cores was ensured by imaging the fiber end faces onto a pyro-camera by means of an aspherical lens. The spectra were recorded with a FTIR-spectrometer.

and 480 fs were focused into the tellurite fibers. The signal pulses were injected into the fibers by means of a 20× aspherical lens objective whereas the idler wavelengths were coupled into the fiber via a 4 mm focal length IR aspherical lens. The resulting total transmission efficiency behind the outcoupling lens (6 mm focal length) depends on the core diameter and was ~35% for the 3.2 μm core fiber, ~40% for the 4.2 μm core fiber, and ~45% for the 5.0 μm core fiber. Furthermore, a wavelength dependence of the transmission losses was observed. The highest transmission efficiencies were achieved at a pump wavelength of 1.7 μm and 2.5 μm. In the wavelength range between 3.0 μm and 4.0 μm the transmission efficiency is nearly constant, decreasing above a wavelength of 4.0 μm. The coupling efficiency is mainly determined by a 5%-10% loss at each IR objective and a Fresnel reflection loss of ~10% at each fiber end face. Additional losses arose due to the NA mismatch of the strong focusing lenses and the fiber. The focal point was adjusted with the aid of an IR-camera (Pyrocam 3, Spiricon) to optimize the beam shape and to ensure single-mode operation. The supercontinuum output was free-space-coupled and analyzed in a Fourier transform infrared spectrometer (Frontier FTIR spectrometer, Perkin Elmer, range 1.2-30 μm).

IV. MEASUREMENT RESULTS

A. Variation of pump wavelength and core diameter

In Figure 3 the spectral broadening characterized in 15 cm long pieces of W-type index tellurite fibers with core diameters of 3.2 μm (a), 4.2 μm (b), and 5.0 μm (c) is displayed for different idler pump wavelengths. The eight pump wavelengths each represented by a different color ranged between 2.6 μm and 4.1 μm. The input powers were kept fixed at 200 mW for each input wavelength

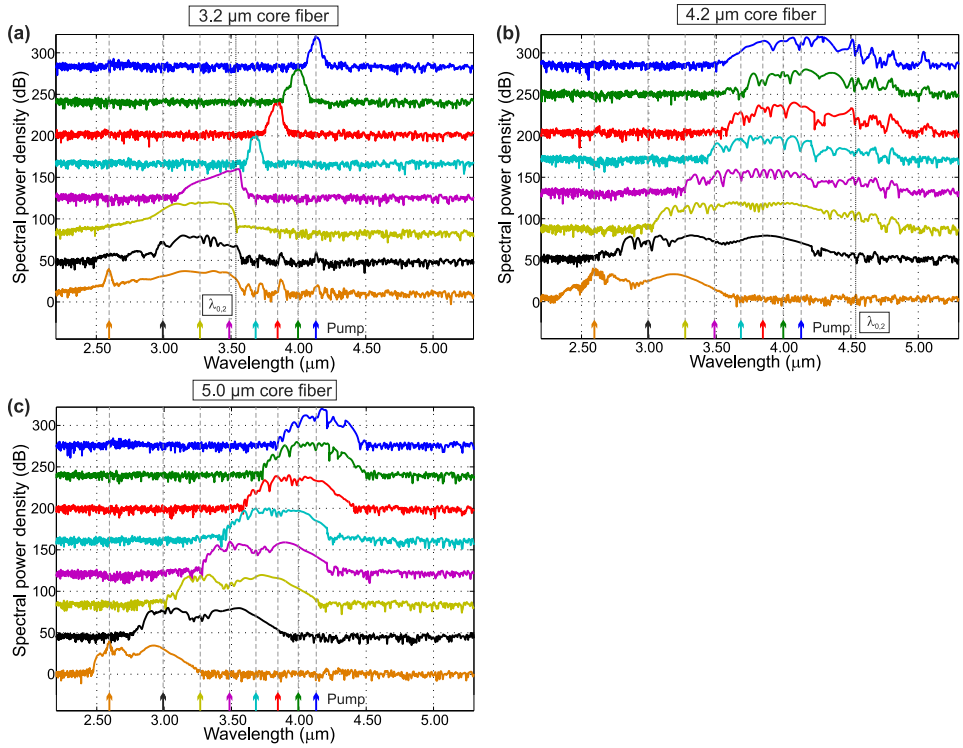

FIG. 3. Spectral broadening of the supercontinuum as a function of launched idler wavelengths (each color corresponds to a certain pump wavelength) at fixed input powers of 200 mW (150 mW at a pump wavelength of 2.6 μm). The fiber lengths are kept fixed at 15 cm. The core diameters are (a) 3.2 μm, (b) 4.2 μm, and (c) 5.0 μm. The position of the second ZDW (marked with a dotted line) has a strong impact on the spectral broadening and can either limit (a) or enhance (b) the bandwidth in comparison to (c). The broadest spectrum with a bandwidth of over 2000 nm has been achieved with a 4.2 μm core diameter fiber when pumped at a wavelength of 3.0 μm (black curve in (b)). The average output powers were between 50 and 85 mW. For better visibility, each spectrum was shifted upwards by 40 dB.

except at 2.6 μm (150 mW) due to lower available power from the OPA. The achieved average output powers behind the out-coupling lens ranged between 50 mW and 85 mW, corresponding to pulse energies between 1.2 nJ and 2.0 nJ. The nonlinear spectral broadening behavior is dramatically influenced by the dispersion properties of the fibers with different core diameters, especially by the position of the second ZDW relative to the pump wavelength. The position of the second ZDW is shifted with increasing core diameter due to the altering strength of waveguide dispersion (see Fig. 1(b)).

For the fiber with a core diameter of 3.2 μm (Fig. 3(a)) we can clearly see a difference in the spectral bandwidth for pump wavelengths below and above the second ZDW. When pumping in the anomalous dispersion regime between the two ZDWs, soliton dynamics lead to spectral broadening (orange to violet curves). Thereby, the soliton self-frequency shift (SSFS) plays a dominant role, shifting spectral components to the long wavelength side. However, a sharp edge forms at the second ZDW stopping the spectral broadening towards the red and resulting in a cancellation of SSFS.[29] The limit in spectral broadening through SSFS is accompanied by the formation of red-shifted DW.[30,31] Energy from the most intense red-shifted soliton located closely below the second ZDW is transferred into red-shifted dispersive waves which are observable as distinctive spectral peaks between 3.6 μm and 4.1 μm in the normal dispersion range of the fiber especially in case of the 2.6 μm pump wavelength. When the fiber is directly pumped in the normal dispersion regime above the second ZDW, the pulse is rapidly temporally broadened due to the large positive dispersion and hence almost no spectral broadening takes place (turquoise to blue curves). However, the pulses were still guided in the fiber core but with an ascending power content in the outer cladding for increasing wavelengths. As a result, optical losses slightly increase already for wavelengths shorter than the leakage cutoff. Furthermore, we obtained a discrepancy between the experimentally observed second ZDW in Fig. 3(a) and the calculated second ZDW (Fig. 1(b)) of around 0.1 μm which can be explained by a slight deviation of the core diameter as also observed in Ref. 32.

In case of the 4.2 μm fiber (Fig. 3(b)) the second ZDW is shifted to about 4.6 μm which enables larger bandwidths. We can pump exclusively in the anomalous dispersion regime between the two ZDWs. So no abrupt breakdown in the spectral broadening is observable as in the former case with the 3.2 μm core fiber. However, a similar spectral feature occurs if the spectral broadening is strong enough to shift components in the vicinity of the second ZDW. Beginning with the 3.0 μm pump wavelength (black curve) the spectral bandwidth is large enough to approach the second ZDW forming DWs in the normal dispersion regime of the fiber. In case of the 4.1 μm pump wavelength spectral peaks appear up to a wavelength of 5.1 μm with a weakly pronounced gap between the second ZDW and the red-shifted DWs. The broadest spectrum could be achieved at a pump wavelength of 3.0 μm with a bandwidth of over 2000 nm, spanning from 2.6 μm up to 4.6 μm. Due to short nonlinear lengths in the range of some centimeters ($L_{\mathrm{NL}} = 1/\gamma P_0$ with the nonlinear coefficient γ, and peak power P_0) soliton propagation dynamics occurred rapidly due to soliton fission already after the first centimeters of propagation along the fiber.

The fiber with a core diameter of 5.0 μm has a second ZDW at around 6.0 μm. Hence, the second ZDW is not reached by the furthest red-shifted soliton resulting in the absence of any red-shifted dispersive waves. The spectral broadening is reduced compared to the 4.2 μm core fiber mainly due to an increased mode area leading to a weaker nonlinearity and enhanced anomalous dispersion. The broadest spectrum covering the spectral range from 2.8 to 3.8 μm is again obtained at a pump wavelength of 3.0 μm.

In general, with short femtosecond pulses and hence high peak power and nonlinearity, no significant peak at the pump wavelength is observed as compared to Ref. 16 with picosecond pulses. This feature shows that the pump beam was efficiently converted into novel spectral components. The power proportion of the supercontinua in the 3-5 μm atmospheric window are very high due to the ability to pump with long idler wavelengths. The sometimes observed dip at around 4.3 μm is due to atmospheric absorption mainly caused by CO_2 due to the free-space-coupling into the FTIR.

The temporal coherence properties of the supercontinuum depend on the relative importance of soliton fission and modulation instabilities as described in Ref. 20. By pumping in the anomalous dispersion regime, shot noise from the pump laser can be amplified by modulation instability, leading to a partial decoherence of the supercontinuum. The coherence properties can be kept at a

high level for a soliton number $N << 16$.[20] The soliton order N is defined as $N = (L_D/L_{NL})^{1/2}$ with the dispersion length $L_D = T_0^2/|\beta_2|$ (pulse width T_0 and dispersion parameter β_2) and the nonlinear length L_{NL}. The coherence properties can be increased for input pulses with a decreased soliton order N. For the fiber and laser parameters used in our experiment the soliton orders range between $N = 10$ and $N = 2$ with a decreasing soliton order for pump wavelengths far from the first zero dispersion wavelength. Hence, the general condition $N << 16$ is satisfied with an expected improvement in the coherence for longer pump wavelengths. A way to maintain the coherence of the pump beam during SC generation process is to use fundamental soliton pump pulses with $N = 1$ rather than high order soliton pulses. A single soliton coherent spectrum could be obtained if we were able to use shorter pulses with a duration of 100 fs in case of the 4.2 μm core diameter fiber at a pump wavelength of 4.0 μm. When pumped in the normal dispersion regime the coherence can be also maintained since modulation instability does not occur.[20]

B. Variation of fiber length

Figure 4 depicts the spectral broadening for two different fiber lengths of 15 cm and 100 cm at pump wavelengths closely below and above the first ZDW which is located at 1.9 μm. The launched pump wavelengths in the 4.2 μm core diameter fiber are 1.7 μm (Fig. 4(a)) and 2.6 μm (Fig. 4(b)). The input pump powers are 300 mW and 150 mW, respectively, resulting in output powers between 130 mW and 60 mW. As shown in the review article of Ref. 20 the supercontinuum characteristic can vary significantly with the position of the input pulse wavelength relative to the fiber ZDW. When pumping the fiber in the normal dispersion regime, symmetrical broadening due to self-phase modulation (SPM) dominated at the initial stage of spectral evolution. However, in case of the 15 cm long fiber energy was transferred to spectral components in the anomalous dispersion regime above 2 μm, resulting in significant spectral broadening due to soliton dynamics. By using the longer fiber of 100 cm the bandwidth could be further enhanced and a flat spectrum spanning from 1.4 to 2.8 μm was obtained.

As the pump wavelength was switched to the anomalous GVD regime an increased spectral width and more distinct soliton peaks were observed. After an initial stage of pulse compression a launched higher order soliton breaks up into a train of fundamental solitons referred to as soliton fission.[20] For the pump wavelength of 2.6 μm soliton fission occurred on a length scale of around 3 cm. The subsequent SSFS broadening mechanism towards the red spectral components is based on Raman scattering. The characteristic propagation distance over which the solitons begin to separate is $\sim 5L_D$.[20] For our parameters the dispersion length was calculated to be 27 cm. Hence, the 100 cm fiber is triple the dispersion length which leads to distinct soliton formation and to a spectral extension from 2.4 to 4.0 μm.

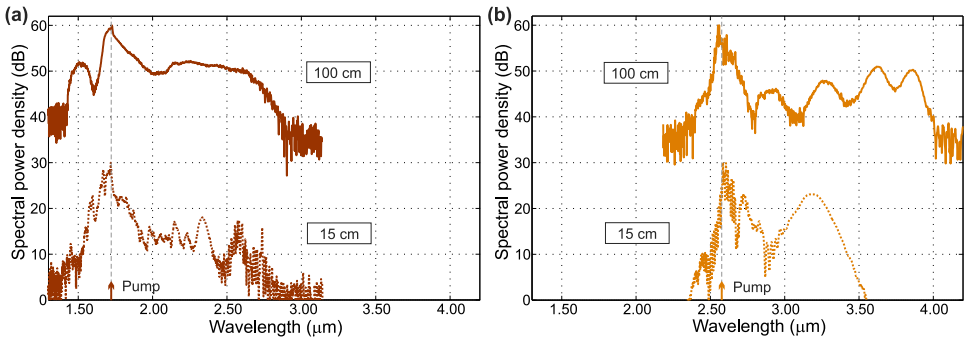

FIG. 4. Spectral broadening of the supercontinuum as a function of fiber length: 100 cm (solid curves) and 15 cm (dotted curves) at fixed input powers. The pump wavelengths (a) 1.7 μm (brown curves) and (b) 2.6 μm (orange curves) were launched closely below and above the first ZDW which is located at ~1.9 μm. The 100 cm long fibers have demonstrated the broader bandwidths for both pump wavelengths due to weak dispersion around the first ZDW and a relatively flat dispersion profile. For better visibility, each spectrum is separated by 30 dB.

Due to the detuning of the pump wavelength from the first ZDW, a gap exists in the supercontinuum spectra between the generated blue-shifted dispersive wave radiation in the normal dispersion range of the fiber at around 1.5 μm and the Raman soliton components. Furthermore, the blue-shifted dispersive wave radiation is very weak due to the enhanced losses at the IR-objectives in that wavelength range and due to the presence of Raman scattering which reduces the energy transfer to the dispersive wave significantly as well.[20] Hence, the continuous detection of the entire spectral range above the noise level of the FTIR-spectrometer of about −30 dB was limited and only the strong Raman soliton components were shown in Fig. 4.

For longer pump wavelengths the most red-shifted solitons reach the second ZDW and the most red-shifted DWs extended up to the transmission edge of tellurite glass already in case of the 15 cm long fiber. Hence, an increase in fiber length will not result in a significant enhancement of spectral broadening.

C. Variation of pump power

The evolution of the supercontinuum spectrum for a 15 cm long fiber with a core diameter of 5.0 μm as a function of input power is displayed in Fig. 5. At low pump power, the spectral broadening was dominated by SPM around the pump wavelength of 3.2 μm. With increased power, higher order soliton fission occurs with a first separated soliton shifted to a wavelength of 3.5 μm. Subsequently, several separated solitons were clearly distinguishable and their red-shift was mainly generated by the Raman based soliton-self-frequency shift due to the strong Raman coefficient of tellurite glass.[33] The expansion of the supercontinuum at the maximum input power of 460 mW is up to a wavelength of 4.6 μm. The achieved output power is 130 mW. Further spectral broadening through SSFS is expected with increased pump power due to the fact that the second ZDW is far-off. However, limiting factors are mainly the finite transmission window of tellurite glass and the increased anomalous dispersion at longer wavelengths. The measured beam profile of the output beam within the wide spectral range appeared to be near TEM_{00} at all pump wavelengths (see inset of Fig. 5), as also observed in Ref. 16. The polarization state of the output was checked for the 4.2 μm and 5.0 μm core fibers with lengths of 15 cm at a pump wavelength of 1.55 μm. The pump was linearly polarized. No instabilities in the polarization state were observed in time as well as at

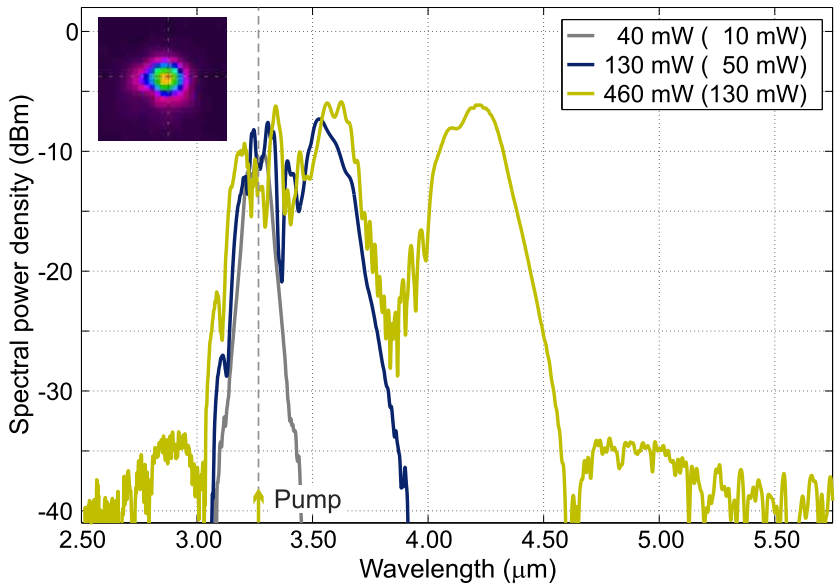

FIG. 5. Spectral evolution of the supercontinuum as a function of input power for the 5.0 μm core fiber at a pump wavelength of 3.2 μm and a fiber length of 15 cm. Red-shifted solitons were the dominant broadening mechanism in the anomalous dispersion regime due to the strong Raman coefficient of tellurite glass which resulted in asymmetric spectral evolution. For the maximum input power of 460 mW, an output power of 130 mW was obtained. Inset: Transversal mode profile.

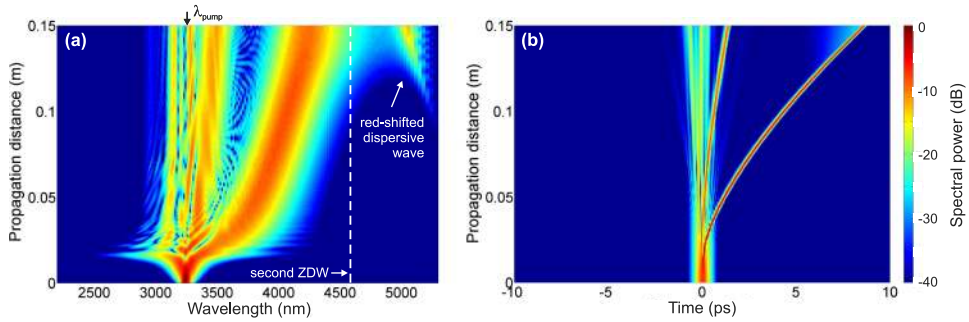

FIG. 6. Numerical simulation of the (a) spectral and (b) temporal evolution in a 15 cm long fiber with a core diameter of 4.2 μm.

increased input powers. However, the fibers show some form-birefringence. The output polarization ratio (power behind polarizer for maximum transmission divided by power behind polarizer rotated by 90°) varies with the angle of the input polarization. In the optimum case, the polarization ratio at the output is 90/10, but when the input polarization is rotated by 45°, the polarization ratio at the output decreases to 60/40. The origin of the birefringence is supposed to result from an elliptical core due to fabrication. The influence on the supercontinuum spectra is negligible. The output power of the supercontinuum is stable and varies at most only by ±3% over an hour.

D. Numerical modeling

The spectral and temporal evolution of pulses launched at a pump wavelength of 3.25 μm in a 4.2 μm core diameter tellurite fiber was calculated by solving the generalized nonlinear Schrödinger equation similar to Ref. 17 to show the qualitative impact of the second ZDW in a W-type index fiber. For the simulation, dispersion coefficients in the Taylor series expansion of the propagation constant are taken up to the 10th order to obtain decent agreement with the dispersion curve plotted in Fig. 1(b). We neglect absorption since the fiber length in the simulation is only 15 cm. The Raman response function of tellurite glass from Refs. 33 and 34 with a Raman fraction of $f_R = 0.34$ and a nonlinear refractive index value of $n_2 = 38 \times 10^{-20}$ m^2/W is used. Simulation results in Fig. 6 confirm the experimentally observed broadening behavior. The same pulse parameters as in the experiment (Section IV A) are used in the numerical study. When pumped in the anomalous dispersion regime, soliton dynamics broadens the spectrum rapidly in the first few centimeters of the fiber as displayed in Fig. 6(a). The soliton fission length[20] $L_{\text{fiss}} \sim L_D/N$ is about 2 cm. Spectral components are shifted to the second ZDW forming a red-shifted dispersive wave in the normal dispersion regime of the fiber.[31] The spectral power density of the dispersive wave in the simulation is overestimated since we neglect material absorption which increases above a wavelength of 4.5 μm.[18]

The temporal feature of the supercontinuum is mainly determined by the residual pump pulse and the fundamental solitons as demonstrated in Fig. 6(b). The first (shortest) soliton has the largest group velocity difference relative to the pump and hence has the largest temporal delay. Since the soliton fission length, as well as the pump pulse duration, increases for longer pump wavelengths (from ~2 cm and 280 fs at 3.0 μm to ~4 cm and 475 fs at 4.1 μm, respectively) the shorter duration solitons that are ejected earlier in the fission process are expected to be temporally further separated for shorter pump wavelengths. For a more sophisticated numerical study the full complexity of the fiber group velocity dispersion and the IR transmission edge of tellurite glass have to be implemented which is not the subject of this paper.

V. CONCLUSION

The variation of the spectral bandwidth was investigated in a low-loss W-type index tellurite fiber by changing the core diameter, pump wavelength, fiber length, and pump power. The pump

source was based on a recently developed post-amplified fiber-feedback optical parametric oscillator which delivered tunable fs-pulses at wavelengths from 1.7 μm to 4.1 μm with 43 MHz repetition rate. We achieved a spectral bandwidth of over 2000 nm spanning from 2.6 to 4.6 μm mainly limited by the long-wavelength edge of the transmission window of tellurite glass. When shifting the second ZDW to wavelengths closely below 5 μm the spectral broadening can benefit from the generation of red-shifted dispersive waves up to a wavelength of 5.1 μm. This is, to the best of our knowledge, the furthest red-shifted DWs in the mid-IR. The position of the second ZDW can be easily and precisely controlled by the core size. This feature was also studied in tapered tellurite microstructured fibers but higher losses in the mid-IR prevented the experimental observation.[14] By pumping a 15 cm long fiber at the appropriate wavelength of 3.0 μm in the anomalous dispersion regime, a supercontinuum with a very high power proportion of 90% in the important transparent atmospheric window between 3 μm and 5 μm can be obtained. This result confirms that ultra-fast mid-infrared pulses around a wavelength of 3 μm are well suited for efficient SC generation as previously proposed in Ref. 17. The excellent mechanical properties of the simple solid-cladding tellurite fiber allow for rather high average output powers of up to 160 mW with the advantage of further power scalability.

ACKNOWLEDGMENTS

This work was supported financially by DFG, BMBF, ERC (Complexplas), Carl-Zeiss-Stiftung, BW-Stiftung, and Alexander von Humboldt Stiftung. We acknowledge support from the open access fund of University of Stuttgart.

[1] J. Swiderski, "High-power mid-infrared supercontinuum sources: Current status and future perspectives," Prog. Quantum Electron. **38**, 189–235 (2014).
[2] A. Schliesser, N. Picqué, and T. W. Hänsch, "Mid-infrared frequency combs," Nat. Photonics **6**, 440–449 (2012).
[3] Y. Yu, X. Gai, T. Wang, P. Ma, R. Wang, Z. Yang, D.-Y. Choi, S. Madden, and B. Luther-Davies, "Mid-infrared supercontinuum generation in chalcogenides," Opt. Mater. Express **3**, 1075–1086 (2013).
[4] G. Tao, H. Ebendorff-Heidepriem, A. M. Stolyarov, S. Danto, J. V. Badding, Y. Fink, J. Ballato, and A. F. Abouraddy, "Infrared fibers," Adv. Opt. Photonics **7**, 379–458 (2015).
[5] A. Lin, A. Zhang, E. J. Bushong, and J. Toulouse, "Solid-core tellurite glass fiber for infrared and nonlinear application," Opt. Express **17**, 16716–16721 (2009).
[6] R. R. Gattass, L. B. Shaw, V. Q. Nguyen, P. C. Pureza, I. D. Aggarwal, and J. S. Sanghera, "All-fiber chalcogenide-based mid-infrared supercontinuum source," Opt. Fiber Technol. **18**, 345–348 (2012).
[7] S. Kedenburg, T. Steinle, F. Mörz, A. Steinmann, and H. Giessen, "High-power mid-infrared high repetition-rate supercontinuum source based on a chalcogenide step-index fiber," Opt. Lett. **40**, 2668–2671 (2015).
[8] U. Møller, Y. Yu, I. Kubat, C. R. Petersen, X. Gai, L. Brilland, D. Mechin, C. Caillaud, J. Troles, B. Luther-Davies, and O. Bang, "Multi-milliwatt mid-infrared supercontinuum generation in a suspended core chalcogenide fiber," Opt. Express **23**, 3282–3291 (2015).
[9] A. Al-kadry, M. E. Amraoui, Y. Messaddeq, and M. Rochette, "Two octaves mid-infrared supercontinuum generation in As_2Se_3 microwires," Opt. Express **22**, 31131–31137 (2014).
[10] W. Yang, B. Zhang, G. Xue, K. Yin, and J. Hou, "Thirteen watt all-fiber mid-infrared supercontinuum generation in a single mode ZBLAN fiber pumped by a 2 μm MOPA system," Opt. Lett. **39**, 1849–1852 (2014).
[11] T. Cheng, L. Zhang, X. Xue, A. Wang, D. Deng, T. Suzuki, and Y. Ohishi, "Broadband cascaded four-wave mixing and supercontinuum generation in a tellurite microstructured optical fiber pumped at 2 μm," Opt. Express **23**, 4125–4134 (2015).
[12] M. Belal, L. Xu, P. Horak, L. Shen, X. Feng, M. Ettabib, D. J. Richardson, P. Petropoulos, and J. H. V. Price, "Mid-infrared supercontinuum generation in suspended core tellurite microstructured optical fibers," Opt. Lett. **40**, 2237–2240 (2015).
[13] I. Savelii, O. Mouawad, J. Fatome, B. Kibler, F. Désévédavy, G. Gadret, J.-C. Jules, P.-Y. Bony, H. Kawashima, W. Gao, T. Kohoutek, T. Suzuki, Y. Ohishi, and F. Smektala, "Mid-infrared 2000-nm bandwith supercontinuum generation in suspended-core microstructured sulfide and tellurite optical fibers," Opt. Express **20**, 27083–27093 (2012).
[14] J. Picot-Clemente, C. Strutynski, F. Amrani, F. Désévédavy, J.-C. Jules, G. Gadret, D. Deng, T. Cheng, K. Nagasaka, Y. Ohishi, B. Kibler, and F. Smektala, "Enhanced supercontinuum generation in tapered tellurite suspended core fiber," Opt. Commun. **354**, 374–379 (2015).
[15] P. Domachuk, N. A. Wolchover, M. Cronin-Golomb, A. Wang, A. K. George, C. M. B. Cordeiro, J. C. Knight, and F. G. Omenetto, "Over 4000 nm bandwidth of mid-IR supercontinuum generation in sub-centimeter segments of highly nonlinear tellurite PCFs," Opt. Express **16**, 7161–7168 (2008).
[16] R. Thapa, D. Rhonehouse, D. Nguyen, K. Wiersma, C. Smith, J. Zong, and A. Chavez-Pirson, "Mid-IR supercontinuum generation in ultra-low loss, dispersion-zero shifted tellurite glass fiber with extended coverage beyond 4.5 μm," Proc. SPIE **8898**, 889808 (2013).
[17] C. Wei, X. Zhu, R. A. Norwood, F. Song, and N. Peyghambarian, "Numerical investigation on high power mid-infrared supercontinuum fiber lasers pumped at 3 μm," Opt. Express **21**, 29488–29504 (2013).
[18] D. L. Rhonehouse, J. Zong, D. Nguyen, R. Thapa, K. Wiersma, C. Smith, and A. Chavez-Pirson, "Low loss, wide transparency, robust tellurite glass fibers for mid-IR (2-5 μm) applications," Proc. SPIE **8898**, 88980D (2013).

[19] J.-C. Gauthier, V. Fortin, J.-Y. Carrée, S. Poulain, M. Poulain, R. Vallée, and M. Bernier, "Mid-IR supercontinuum from 2.4 to 5.4 μm in a low-loss fluoroindate fiber," Opt. Lett. **41**, 1756–1759 (2016).
[20] J. M. Dudley, G. Genty, and S. Coen, "Supercontinuum generation in photonic crystal fiber," Rev. Mod. Phys. **78**, 1135–1184 (2006).
[21] S. Kawakami and S. Nishida, "Characteristics of a doubly clad optical fiber with a low-index inner cladding," IEEE J. Quantum Electron. **10**, 879–887 (1974).
[22] J. A. Buck, in *Fundamentals of Optical Fibers* (Wiley, 2004), Chap. 6.
[23] L. G. Cohen, D. Marcuse, and W. L. Mammel, "Radiating leaky-mode losses in single-mode lightguides with depressed-index claddings," IEEE J. Quantum Electron. **18**, 1467–1472 (1982).
[24] M. Monerie, "Propagation in doubly clad single-mode fibers," IEEE J. Quantum Electron. **18**, 535–542 (1982).
[25] A. Steinmann, B. Metzger, R. Hegenbarth, and H. Giessen, in *Conference on Lasers and Electro-Optics, OSA Technical Digest (CD)* (Optical Society of America, 2011), paper CThAA5.
[26] T. Steinle, F. Neubrech, A. Steinmann, X. Yin, and H. Giessen, "Mid-infrared Fourier-transform spectroscopy with a high-brilliance tunable laser source: Investigating sample areas down to 5 μm diameter," Opt. Express **23**, 11105–11113 (2015).
[27] T. Südmeyer, J. Aus der Au, R. Paschotta, U. Keller, P. G. R. Smith, G. W. Ross, and D. C. Hanna, "Femtosecond fiber-feedback optical parametric oscillator," Opt. Lett. **26**, 304–306 (2001).
[28] F. Mörz, T. Steinle, A. Steinmann, and H. Giessen, "Multi-Watt femtosecond optical parametric master oscillator power amplifier at 43 MHz," Opt. Express **23**, 23960–23967 (2015).
[29] D. V. Skryabin, F. Luan, J. C. Knight, and P. St. J. Russell, "Soliton self-frequency shift cancellation in photonic crystal fibers," Science **301**, 1705–1708 (2003).
[30] W. Wang, H. Yang, P. Tang, C. Zhao, and J. Gao, "Soliton trapping of dispersive waves in photonic crystal fiber with two zero dispersive wavelengths," Opt. Express **21**, 11215–11226 (2013).
[31] S. Zhao, H. Yang, N. Chen, X. Fu, and C. Zhao, "Soliton trapping of dispersive waves in photonic crystal fiber with three zero-dispersive wavelengths," IEEE Photon. J. **7**, 7102709 (2015).
[32] B. Kibler, C. Finot, G. Gadret, G. Millot, J. Wojcik, M. Szpulak, and W. Urbanczyk, "Second zero dispersion wavelength measurement through soliton self-frequency shift compensation in suspended core fibre," Electron. Lett. **44**, 1370–1371 (2008).
[33] X. Yan, G. Qin, M. Liao, T. Suzuki, and Y. Ohishi, "Transient Raman response and soliton self-frequency shift in tellurite microstructured fiber," J. Appl. Phys. **108**, 123110 (2010).
[34] D. Hollenbeck and C. D. Cantrell, "Multiple-vibration-mode model for fiber-optic Raman gain spectrum and response function," J. Opt. Soc. Am. B **19**, 2886–2892 (2002).